

An Asymmetric Distance Model for Cross-View Feature Mapping in Person Reidentification

Ying-Cong Chen, Wei-Shi Zheng, Jian-Huang Lai, and Pong C. Yuen

Abstract—Person reidentification, which matches person images of the same identity across nonoverlapping camera views, becomes an important component for cross-camera-view activity analysis. Most (if not all) person reidentification algorithms are designed based on appearance features. However, appearance features are not stable across nonoverlapping camera views under dramatic lighting change, and those algorithms assume that two cross-view images of the same person can be well represented either by exploring robust and invariant features or by learning matching distance. Such an assumption ignores the nature that images are captured under different camera views with different camera characteristics and environments, and thus, mostly there exists large discrepancy between the extracted features under different views. To solve this problem, we formulate an asymmetric distance model for learning camera-specific projections to transform the unmatched features of each view into a common space where discriminative features across view space are extracted. A cross-view consistency regularization is further introduced to model the correlation between view-specific feature transformations of different camera views, which reflects their nature relations and plays a significant role in avoiding overfitting. A kernel cross-view discriminant component analysis is also presented. Extensive experiments have been conducted to show that asymmetric distance modeling is important for person reidentification, which matches the concerns on cross-disjoint-view matching, reporting superior performance compared with related distance learning methods on six publically available data sets.

Index Terms—Cross-view matching, person reidentification, visual surveillance.

I. INTRODUCTION

NOWADAYS, camera network has been widely deployed in public infrastructure such as airports, railway stations, and hospitals for surveillance. Due to economic issues, there are always nonoverlapping fields between camera views. It then challenges tracking of people and activity prediction over nonoverlapping camera networks. Hence, it is critical to reidentify a target person when he/she reappears in another camera view. Such a problem is called the *person reidentification*.

However, appearance of a pedestrian would dramatically change across camera views because the environment and camera orientations can be totally different. There are two main feature discrepancy problems: 1) the view-wise discrepancy and 2) the pedestrian-wise discrepancy. The view-wise discrepancy is caused by environmental changes such as illumination and the white balance of camera, and the pedestrian-wise discrepancy is caused by the pedestrian himself/herself such as those with backpacks or unzipped jackets, as well as significant pose changes [see Fig. 2(a) and (b)].

Alleviating the appearance changes across nonoverlapping camera views includes: 1) seeking discriminative and robust image descriptor [2]–[4]; 2) learning reliable distance/subspace models [5]–[9]; and 3) preprocessing model such as histogram equalization [2], [3] and bright transfer model [10]–[12]. The first two approaches implicitly assume that one can select a set of features that do not change dramatically. However, appearance could vary dramatically due to indoor/outdoor lighting and pose variations. As such, images of the same person from different camera views will look quite different. Although distance learning methods try to select features robust to those changes, most of these features are extracted based on appearance, especially color features [13] that would be largely affected by illumination or camera characteristics (e.g., white balance). However, the existing methods on using distance learning in person reidentification are all focused on symmetric modeling, i.e., most of them are based on the following distance form between any two samples \mathbf{x}_i and \mathbf{x}_j :

$$\begin{aligned} d(\mathbf{x}_i, \mathbf{x}_j) &= \sqrt{(\mathbf{x}_i - \mathbf{x}_j)^T \mathbf{M} (\mathbf{x}_i - \mathbf{x}_j)} \\ &= \|\mathbf{U}^T \mathbf{x}_i - \mathbf{U}^T \mathbf{x}_j\|_2 \end{aligned} \quad (1)$$

Manuscript received May 9, 2015; revised October 10, 2015; accepted December 23, 2015. Date of publication January 6, 2016; date of current version August 2, 2017. This work was supported in part by the Computational Science Innovative Research Team Program, Guangdong Provincial Government of China, in part by the Natural Science Foundation of China under Grant 61472456, Grant 61522115, Grant 61573387, and Grant 6151101169, in part by the Guangzhou Pearl River Science and Technology Rising Star Project under Grant 2013J2200068, in part by the Guangdong Natural Science Funds for Distinguished Young Scholar under Grant S2013050014265, in part by the Guangdong Program under Grant 2015B010105005, and in part by the Hong Kong RGC General Research Fund under Grant HKBU 12202514. This paper was recommended by Associate Editor C. Shan. (Corresponding author: Wei-Shi Zheng.)

Y.-C. Chen is with the School of Electronics and Information Technology, Sun Yat-sen University, Guangzhou 510275, China (e-mail: chyngc@mail2.sysu.edu.cn).

W.-S. Zheng is with the School of Data and Computer Science, Sun Yat-sen University, Guangzhou 510275, China, also with the Guangdong Provincial Key Laboratory of Computational Science, Guangzhou 510275, China, and also with the Collaborative Innovation Center of High Performance Computing, National University of Defense Technology, Changsha 410073, China (e-mail: wszheng@ieee.org).

J.-H. Lai is with the School of Data and Computer Science, Sun Yat-sen University, Guangzhou 510275, China, and also with the Guangdong Key Laboratory of Information Security Technology, Guangzhou 510275, China (e-mail: stsljh@mail.sysu.edu.cn).

P. C. Yuen is with the Department of Computer Science, Hong Kong Baptist University, Hong Kong (e-mail: pcyuen@comp.hkbu.edu.hk).

Color versions of one or more of the figures in this paper are available online at <http://ieeexplore.ieee.org>.

Digital Object Identifier 10.1109/TCSVT.2016.2515309

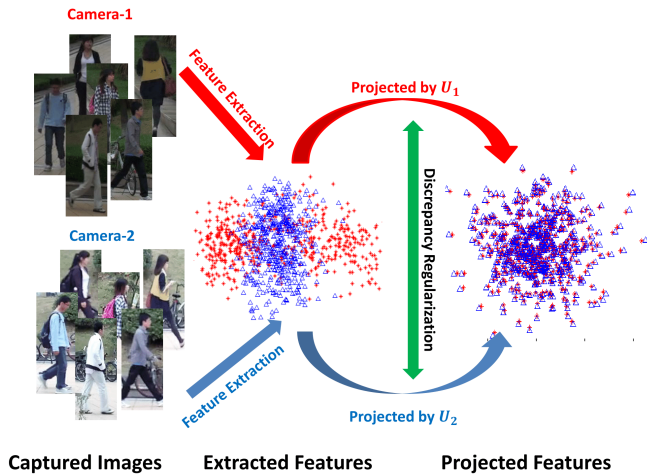


Fig. 1. Illustration of cross-view feature discrepancy problem and our method. These images are selected from the SYSU data set [1]. After feature extraction, we perform principal component analysis for visualization. It shows that the extracted features are highly divergent so that the distributions of person images of two views are very distinct and thus, reidentification is extremely difficult. Our method seeks for good view-specific mappings that project the original feature to a common space and make reidentification more reliable. After the feature projection induced by the proposed asymmetric distance model, the person images of two views are more likely to match. To model the correlation nature of different projections, a consistency regularization is imposed to restrict the difference in the projections.

where the positive semidefinite matrix \mathbf{M} is factorized into $\mathbf{M} = \mathbf{U}\mathbf{U}^T$.¹ The symmetric modeling intrinsically assumes that the same feature transformation is applied to all the camera views, and this ignores feature discrepancy caused by the different nature of images captured under different camera views. Since there exists a feature discrepancy problem across nonoverlapping camera views due to view-wise and pedestrian-wise discrepancies, the conventional unitary projection matrix learning in existing distance/subspace learning methods [5]–[7], [16]–[21] could discard those features with large discrepancy that may be discriminant during the cross-view matching. Section III-A will give the details of this analysis.

In this paper, we propose an asymmetric distance model for person reidentification, i.e., we generalize the symmetric form in (1) and take the view label into account by considering the model based on the following asymmetric form:

$$d(\{\mathbf{x}_i^p, p\}, \{\mathbf{x}_j^q, q\}) = \|\mathbf{U}^{pT} \mathbf{x}_i^p - \mathbf{U}^{qT} \mathbf{x}_j^q\|_2 \quad (2)$$

where p and q are the labels of two different camera views and always $\mathbf{U}^p \neq \mathbf{U}^q$. Essentially speaking, we form the asymmetric learning through learning \mathbf{U}^p and \mathbf{U}^q , which we call the cross-view feature transformation. We hold an assumption that one can seek a latent common space such that the extracted features across different camera views for the same person become more similar, meanwhile for different persons, they become more dissimilar. Based on this assumption,

¹Conventionally, some works such as [5] and [14] directly learn \mathbf{M} under the positive semidefinite constraint, and others like [6] and [15] learn \mathbf{U} , where the learned distance is equivalent to the Euclidean distance of the transformed features. As such, \mathbf{U} can be viewed as extracting robust and discriminative transform from the original input space.

we develop a supervised asymmetric distance learning model. We also observe that albeit discrepancy exists across disjoint camera views, there could exist relation between the contents captured by any two camera views, because of the existence of the same person to match and probably similar indoor/outdoor environments. Hence, the discrepancy between feature transformations \mathbf{U}^p and \mathbf{U}^q should be controlled. To this end, we introduce a cross-view consistency regularization into the cross-view model in order to constrain the difference in view-specific projections, so as to implicitly embed the relation between cross-view images into the distance learning model. Based on the above ideas, we develop a new cross-view matching algorithm for person reidentification, called the cross-view discriminant component analysis, which is illustrated in Fig. 1.

In summary, this paper makes the following contributions.

- 1) We propose and develop a new asymmetric distance learning model, called the CVDCA algorithm, to transform the features under different views to a common space for person reidentification. The proposed method addresses the feature discrepancy problem by view-specific mappings and models the correlation of different views by a consistency regularization. We also experimentally show that this asymmetric distance model performs much better than the symmetric ones.
- 2) The linear CVDCA is further extended to kernel version and kernelized CVDCA is then proposed.

Extensive experiments have been conducted to demonstrate that the proposed CVDCA and Kernel Cross-View Discriminant Component Analysis (KCVDCA) can address the feature discrepancy problem in person reidentification much better.

II. RELATED WORK

In order to obtain robust and discriminative representation of pedestrians across different camera views, various methods were proposed to extract color or texture features. Zhao *et al.* [3], [22] proposed salience-based approaches for person reidentification in which patch matching is employed with adjacency constraint to handle the pose misalignment problem. Later, Zhao *et al.* [2] proposed a midlevel filter that automatically discovers patch clusters. However, since color features are used in patch matching, this processing may not be optimal when illumination of different views varies dramatically. Yang *et al.* [4] proposed a novel salient color-name-based color descriptor (SCNCD) for person reidentification. However, such a descriptor may be divergent of each view if the lighting of different camera views differs to an extent. Kviatkovsky *et al.* [23] proposed an illumination-invariant color feature based on log-chromaticity color space and shape context. However, this method highly depends on high-quality mask, which is usually unavailable in real-world applications. There exist color calibration methods [10]–[12] that aim at learning bright transfer functions to establish a mapping of brightness value between two camera views, and thus the gap between them is reduced. However, the cross-camera-view discrepancy is not only caused by lighting. In addition, because of incomplete ranges of color value

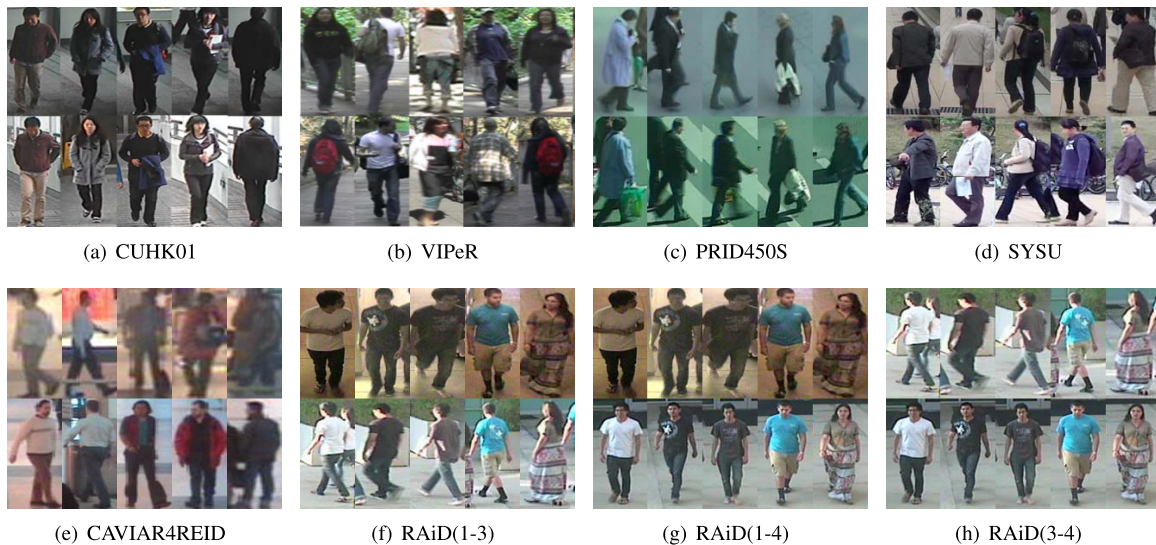


Fig. 2. Typical examples of the data sets and sample pairs with view-wise discrepancy or pedestrian-wise discrepancy. Images of the first row were captured by camera *a* and while images of the second row were captured by camera *b*. (a) Image pairs whose disagreement is more caused by the environmental changes. (b) Images whose disagreement is caused mainly by the pedestrian himself/herself. (c)–(h) Images whose disagreement is caused by both pedestrian himself and environmental changes.

found in the training data, the mapping function may contain many-to-one color correspondence [11], which would cause the loss of useful information. Another approach to deal with the histogram feature mismatch problem is feature warps (FWs) [24]. warp functions are solved by aligning the feature histograms between the two camera views, and then they are used as image pair descriptors. Note that this method uses the principles of dynamic time warping to align histograms of each image pair, which implicitly assumes that the divergence of histograms results from histogram shifting.

Due to the difficulty of designing reliable image descriptors across different camera views, some distance/subspace learning methods have been proposed to reduce the variation across views. Zheng *et al.* [8] formulated person reidentification as a relative distance comparison learning problem by maximizing the probability that relevant samples have smaller distance than the irrelevant ones. Liao and Li [25] proposed a logistic metric learning approach with Positive Semidefinite constraint and an asymmetric sample weighting strategy. Li *et al.* [18] proposed a locally adaptive decision function (LADF) to jointly learn the distance matrix and the locally adaptive threshold. Kostinger *et al.* [17] proposed a simple and effective distance learning called KISS (keep it simple and straightforward) Metric Learning (KISSME) to conduct hypothesis test on similar/dissimilar pairs. Later, Tao *et al.* [26] improved KISSME by introducing a minimum classification criterion and a smoothing technique in order to better estimate the small eigenvalue of the covariance matrix. Liao *et al.* [27] proposed the cross-view quadratic discriminant analysis that has the similar idea of KISSME but can jointly learn a low-dimensional subspace and a metric. Mignon and Jurie [6] proposed Pairwise Constrained Component Analysis (PCCA) to learn a projection with sparse pair-wise similarity/dissimilarity constraints. Later, Xiong *et al.* [28] proposed the regularized PCCA to maximize the inter-class margin and avoid overfitting. Pedagadi *et al.* [9] applied local Fisher discriminant analysis (LFDA) to project

the raw features to a discriminative subspace so that the between-class separability is maximized while the multi-modality structure is preserved and a nonlinear extension using the kernel trick of this work was reported in [28]. Paisitkriangkrai *et al.* [29] proposed a structural learning framework to combine multiple prelearned distances, which leads to better performance than using a unitary distance measure. All these methods are symmetric based, and the underlying assumption of the above methods is that features of all camera views have the same properties, while for person reidentification images captured from different camera views could differ notably. Therefore, the unitary projection matrix shared by all views learned by these methods would probably discard the use of divergent features. Recently, sparse-reconstruction-based classification of face has been extended to person reidentification [30], [31]. However, the reconstruction has an underlying assumption that images of the same person should distribute similarly at different camera views, which is not the fact as shown in this work.

Domain adaptation [32]–[34], which can reduce the gap between different distributions, seems an alternative solution to cross-view matching. However, those methods cannot be an optimal way to diminish the gap between the two camera views in person reidentification, since they assume the existence of overlapping between training and gallery/testing classes, so that the classifier/metric learned from the training set can be adapted to the gallery/testing one, while for person reidentification, there is no overlapping between the training and gallery/testing classes. Note that our work is also different from cross-data set transfer [35]–[37] since we do not incorporate any source data set.

There are related works [39]–[44] in person reidentification that can also learn view-specific mappings. An *et al.* [39], [40] generated a new representation by projecting all samples to the regularized canonical correlation analysis (rCCA) subspace and constructing the reference descriptors with the

reference set. An *et al.* also proposed robust canonical correlation analysis (ROCCA) [41] to better estimate the data covariance matrices. rCCA and ROCCA are multimodal learning methods that project heterogeneous features to a common space and thus they are related to our model. However, the person reidentification we discuss in this paper is not a multimodal learning problem and there are important differences between our method and rCCA or ROCCA. First, rCCA and ROCCA do not control the discrepancy between view-specific feature transformations. Although the feature transformation is specific to each camera view, there should be relation between them, because samples captured from different views are not heterogeneous but related either from the same identity or from people with a similar appearance. As shown in our experiment, this is one of the key factors that makes our model work much better than rCCA. Second, rCCA and ROCCA do not consider intra-view modeling, which is also useful in our problem. In comparison, our method includes cross-view consistency regularization and intra-view modeling. Besides, we introduce local weighting to the feature transformation processing so as to reduce the impact of extremely different positive sample pairs. Hence, our model is more suitable for person reidentification. Liu *et al.* [42] proposed to learn individual local feature projection for each image sample, which intends to alleviate the influence of configuration variations. In addition, Li and Wang [43] proposed to use a gating network to partition the image space of the two camera views into subregions, and some local experts are trained to align the features in the subregions. Some other multimodality methods like cross-modal metric learning (CMML) [45] are related to our approach since they also learn view-specific mappings. However, like rCCA and ROCCA, these methods discussed above do not control the discrepancy of inter-view projections or do not incorporate intra-view modeling, which may not be optimal when applying to person reidentification.

III. APPROACH

A. Feature Discrepancy of Different Camera Views

Let us consider a general case that there are N ($N \geq 2$) cameras with significant feature discrepancy. Let $\mathbf{X}^k = [\mathbf{x}_1^k, \mathbf{x}_2^k, \dots, \mathbf{x}_{n^k}^k] \in \mathbb{R}^{d \times n^k}$ denote the feature matrices extracted from the pedestrian images captured by the k th view, where d is the feature dimension and n^k is the number of samples of the k th view. The average intra-class variation δ and its lower bound δ' of two specific views (views a and b) are given by

$$\begin{aligned} \delta &= \frac{1}{n_p^{a,b}} \sum_{i,j \in \zeta^{a,b}} |\mathbf{x}_i^a - \mathbf{x}_j^b| \\ &\geq \frac{1}{n_p^{a,b}} \sum_{i,j \in \zeta^{a,b}} (\mathbf{x}_i^a - \mathbf{x}_j^b) = \delta' \end{aligned} \quad (3)$$

where $\zeta^{a,b}$ is the set of all positive pairs in views a and b and $n_p^{a,b}$ is the cardinality of $\zeta^{a,b}$.

Let us consider a single-shot situation, i.e., each pedestrian has only one image for each view with $n^a = n^b$. Then δ' can

be rewritten as

$$\delta' = \frac{1}{n_p^{a,b}} \sum_{i=1}^{n^a} \mathbf{x}_i^a - \frac{1}{n_p^{a,b}} \sum_{j=1}^{n^b} \mathbf{x}_j^b. \quad (4)$$

Assume that \mathbf{X}^a and \mathbf{X}^b are histogram features. We draw $(1/n_p^{a,b}) \sum_i \mathbf{x}_i^a$, $(1/n_p^{a,b}) \sum_j \mathbf{x}_j^b$ and δ' in the first and second rows of Fig. 3. We observe that $(1/n_p^{a,b}) \sum_i \mathbf{x}_i^a$ and $(1/n_p^{a,b}) \sum_j \mathbf{x}_j^b$ are not identical, i.e., some features are highly divergent. Those highly different features (the red bars) will generate a high δ' . Note that if \mathbf{X}^a and \mathbf{X}^b are drawn from identical distribution, $(1/n_p^{a,b}) \sum_i \mathbf{x}_i^a$ and $(1/n_p^{a,b}) \sum_j \mathbf{x}_j^b$ shall be similar. Therefore, we believe that such highly different features between the two views are caused by the unmatched distributions, which will lead to the feature discrepancy problem.

Most supervised subspace/metric learning methods try to reduce the intra-class variation and the lower bound δ' will also be reduced. If a method learns an identical projection or distance matrix for all views, the weights of the divergent features tend to be reduced since those features will cause high intra-class variation. As shown in row 6 of Fig. 3, taking LFDA [9], for example, it learns unitary projection for both views, and thus the weights for highly divergent features are relatively small. However, those features could contain some discriminative information, and deemphasizing them may result in a performance drop. Since using a unitary mapping for all views is not optimal to extract discriminative features, we propose to learn camera-view specific mappings. The camera-view specific mappings are learned so as to transform those features into a common space. As shown in the third and fourth rows of Fig. 3, using view-specific mappings, the weights on highly divergent features do not have to be suppressed and more features can be used. By learning view specific transforms, we ultimately formulate an asymmetric distance model called CVDCA for matching person images across disjoint camera views.

To provide a further analysis of the discrimination power of symmetric and asymmetric distances, we quantify the power by computing the quotient between the average inter-class distance and the average intra-class distance based on the features generated by CVDCA and LFDA. The quotient is defined as follows:

$$Q = \frac{\sum_{i,j \in \bar{\zeta}^{a,b}} \|\mathbf{y}_i^a - \mathbf{y}_j^b\|^2}{\sum_{i,j \in \zeta^{a,b}} \|\mathbf{y}_i^a - \mathbf{y}_j^b\|^2} \quad (5)$$

where \mathbf{y}_i^a and \mathbf{y}_j^b are projected features, $\bar{\zeta}^{a,b}$ is the set of all negative pairs in views a and b , and $\zeta^{a,b}$ is the set of all positive pairs. Here Q represents the quotient. A larger Q indicates that the features can be separated better and thus they are more discriminative. Note that the values of Q of the features extracted by CVDCA are 1.47, 2.27, and 1.37 for RGB, HSV, YCbCr, respectively, while those extracted by LFDA are 1.10, 1.07, and 1.15, respectively. Therefore, we claim that using view-specific mappings, more discriminative features are retained. In addition, as shown in our experiments,

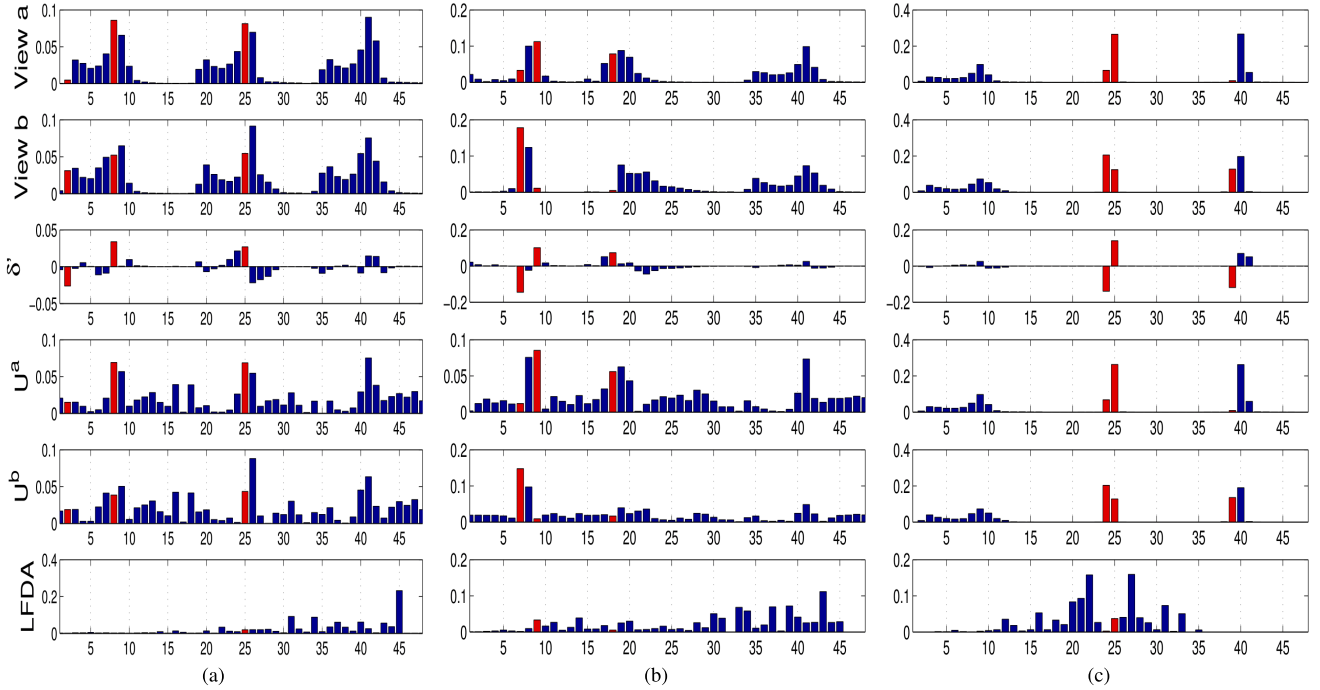


Fig. 3. Example of feature discrepancy of RGB, HSV, and YCbCr features. The first and the second rows show the distributions of $(1/n_p^{a,b}) \sum_i x_i^a$ and $(1/n_p^{a,b}) \sum_j x_j^b$, respectively. The x -axis is the index of bucket and the y -axis is the probability. The third row shows the distribution of δ' . The fourth and fifth rows show view-specific mappings of views a and b trained by our method (will be presented in Section III-B). The sixth row shows the unitary mapping trained by LFDA [9]. The x -axis corresponds to the buckets in the histogram and the y -axis is the weight of each bucket. The yellow bars indicate those features with large δ' . As shown, the unitary mapping learned by LFDA tends to suppress the weight of the highly divergent features, while our method can utilize those features. This experiment was conducted on PRID450S [38]. Best viewed in color. (a) RGB. (b) HSV. (c) YCbCr.

the proposed method does not dismiss the use of these features and achieves a much better performance than LFDA.

B. Discrepancy Reduction by View-Specific Transformations

The asymmetric distance model based person reidentification is formulated by learning feature transformations for each camera view. Let $U^p = [u_1^p, u_2^p, \dots, u_C^p]$ denote the projection matrices for view p , where $p = 1, 2, \dots, N$ and C is the dimension of the projected space. We aim at learning U^p that embeds the features X^p into a discriminative common Euclidean space, where the relevant pairs are expected to be with small Euclidean distances and the irrelevant pairs are with large ones.

It is expected that the learned latent common space could model the relations of both cross-view sample pairs and intra-view sample pairs. Hence, our model consists of both cross-view modeling and intra-view modeling

$$f = f_{\text{cross}} + \eta f_{\text{intra}} \quad (6)$$

where the cross-view modeling f_{cross} and the intra-view modeling f_{intra} can be formulated as the following and η is a positive value that controls the weight of intra-view modeling:

$$f_{\text{cross}} = \sum_{p=1}^{N-1} \sum_{q=p+1}^N \sum_{i=1}^{n^p} \sum_{j=1}^{n^q} \mathbf{W}_{ij}^{p,q} \|U^{pT} x_i^p - U^{qT} x_j^q\|_2^2 \quad (7)$$

$$f_{\text{intra}} = \sum_{p=1}^N \sum_{i=1}^{n^p} \sum_{j=1}^{n^p} \mathbf{W}_{i,j}^{p,p} \|U^{pT} x_i^p - U^{pT} x_j^p\|_2^2. \quad (8)$$

In the above modeling, $\mathbf{W}_{ij}^{p,q}$ is the weight on each pair of samples between views p and q and U^p is a projection of

view p . We define $\mathbf{W}_{ij}^{p,q}$ as

$$\mathbf{W}_{ij}^{p,q} = \begin{cases} \frac{1}{n_{\text{pos}}^{p,q}} \mathbf{A}_{ij}^{p,q} & \text{if } (x_i^p, x_j^q) \in \mathcal{C}^{p,q} \\ -\gamma \frac{1}{n_{\text{neg}}^{p,q}} & \text{otherwise} \end{cases} \quad (9)$$

where $\mathbf{A}_{ij}^{p,q}$ could set as a local weighting term like LFDA [9] or simply set as 1, $n_{\text{pos}}^{p,q}$ and $n_{\text{neg}}^{p,q}$ are the numbers of positive and negative pairs between view p and q , respectively, and γ is a scalar. Since the number of positive pairs is much smaller than the number of negative pairs, we use $(1/n_{\text{pos}}^{p,q})$ and $(1/n_{\text{neg}}^{p,q})$ to normalize them, and thus the weight of intra-class modeling and inter-class modeling can be easily modeled by γ . In this way, minimizing the objective function f will reduce the intra-class difference, meanwhile it will enlarge the inter-class difference. When $p \neq q$, $\mathbf{W}^{p,q}$ characterizes the cross-view relationship; when $p = q$, it characterizes the intra-view relationship.

In order to avoid trivial solution, namely, $U^k = \mathbf{0}$ for $k = 1, 2, \dots, N$, we additionally incorporate some constraints and formulate an optimization problem as

$$\begin{aligned} \min_{U^1, U^2, \dots, U^N} & \sum_{p=1}^{N-1} \sum_{q=p+1}^N \sum_{i=1}^{n^p} \sum_{j=1}^{n^q} \mathbf{W}_{ij}^{p,q} \|U^{pT} x_i^p - U^{qT} x_j^q\|_2^2 \\ & + \sum_{p=1}^N \sum_{i=1}^{n^p} \sum_{j=1}^{n^p} \mathbf{W}_{i,j}^{p,p} \|U^{pT} x_i^p - U^{pT} x_j^p\|_2^2 \\ \text{s.t. } & U^k T M^k U^k = \mathbf{I}, \quad k = 1, 2, \dots, N \end{aligned} \quad (10)$$

where $\mathbf{M}^k = \mathbf{X}^k \mathbf{X}^{kT} + \mu \mathbf{I}$ and \mathbf{I} denotes the identity matrix that avoids singularity of the covariance matrix. These constraints ensure that the projected features of each view have unit amplitude and thus they are not shrunken to zero.

C. Transformations Constrained by Cross-View Consistency Regularization

Intuitively, if the feature distributions of two views are similar, the learned feature transformations \mathbf{U}^p and \mathbf{U}^q are also similar; otherwise, the learned \mathbf{U}^p and \mathbf{U}^q will be different. Since the features of corrupted positive pairs are arbitrarily different, e.g., frontal view and dorsal view of a pedestrian wearing a white t-shirt and a black backpack (see Fig. 2), it could make the learned \mathbf{U}^p and \mathbf{U}^q quite different. These largely different projection basis pairs do not capture the natural property that images from different camera pairs are correlated to an extent, and the performance would drop dramatically when using these projection pairs.

To embed this correlation nature to our model, we propose to penalize those largely different feature transformations. Specifically, the difference in each projection basis pair can be measured by the Bregman discrepancy [46], [47]. Given a strictly convex function $\mathcal{F} : \mathbb{R}^{d \times C} \rightarrow \mathbb{R}$, the Bregman discrepancy of a projection pair is given by

$$d_{\mathcal{F}}(\mathbf{U}^p, \mathbf{U}^q) = \mathcal{F}(\mathbf{U}^p) - \mathcal{F}(\mathbf{U}^q) - \nabla \mathcal{F}(\mathbf{U}^q)^T (\mathbf{U}^p - \mathbf{U}^q) \quad (11)$$

where $\nabla \mathcal{F}$ is the derivative of \mathcal{F} . For any strictly convex \mathcal{F} , $d_{\mathcal{F}}(\mathbf{U}^p, \mathbf{U}^q) \geq 0$.

The choice of \mathcal{F} is nontrivial to the performance and the computational complexity. If we set $\mathcal{F}(\mathbf{x}) = \mathbf{x}^T \mathbf{x}$, the Bregman discrepancy can be simplified to an Euclidean distance $\|\mathbf{U}^p - \mathbf{U}^q\|_F^2$. As will be shown later, such a regularization term results in an elegant solution and it works empirically well. For all camera pairs, $\sum_{p=1}^{N-1} \sum_{q=p+1}^N \|\mathbf{U}^p - \mathbf{U}^q\|_F^2$ is added to the objective function (6). We call this regularization the *cross-view consistency regularization*. In the Appendix, we will explain how this regularization term is related to the prior knowledge of the projection matrices.

Since $\sum_{p=1}^{N-1} \sum_{q=p+1}^N \|\mathbf{U}^p - \mathbf{U}^q\|_F^2 = (N-1) \text{tr}(\sum_{k=1}^N \mathbf{U}^{kT} \mathbf{U}^k - 2 \sum_{p=1}^{N-1} \sum_{q=p+1}^N \mathbf{U}^{pT} \mathbf{U}^q)$, where $\text{tr}(\cdot)$ denotes the trace operation, we formulate a regularized version of (10) as

$$\begin{aligned} \min_{\mathbf{U}^1, \mathbf{U}^2, \dots, \mathbf{U}^N} & \sum_{p=1}^{N-1} \sum_{q=p+1}^N \sum_{i=1}^{n^p} \sum_{j=1}^{n^q} \mathbf{W}_{ij}^{p,q} \|\mathbf{U}^{pT} \mathbf{x}_i^p - \mathbf{U}^{qT} \mathbf{x}_j^q\|_2^2 \\ & + \sum_{p=1}^N \sum_{i=1}^{n^p} \sum_{j=1}^{n^p} \mathbf{W}_{i,j}^{p,p} \|\mathbf{U}^p \mathbf{x}_i^{pT} - \mathbf{U}^p \mathbf{x}_j^{pT}\|_2^2 \\ & + \text{tr} \left(\lambda \sum_{k=1}^N \mathbf{U}^{kT} \mathbf{U}^k - 2\lambda' \sum_{p=1}^{N-1} \sum_{q=p+1}^N \mathbf{U}^{pT} \mathbf{U}^q \right) \\ \text{s.t. } & \mathbf{U}^{kT} \mathbf{M}^k \mathbf{U}^k = \mathbf{I}; \quad k = 1, 2, \dots, N \end{aligned} \quad (12)$$

where

$$\lambda = (N-1)\lambda'. \quad (13)$$

This cross-view consistency regularization is important to exploit the intrinsic nature relations between view-specific feature transformations and help alleviate overfitting significantly, as evaluated in Section IV-D1. We call the above model as CVSDCA.

D. Kernel Extension

The above method learns linear projection matrices for feature transformation and may suffer from the nonlinearity of given data. We further propose the kernel extension to alleviate this problem.

The implicit high-dimensional subspace bases of the k th view could be represented as $\tilde{\mathbf{X}} \boldsymbol{\alpha}^k$, where $\tilde{\mathbf{X}}$ is the high-dimensional column-wise feature matrix of all training data. Therefore, the projected data could be represented as

$$h^k(\tilde{\mathbf{x}}^k) = \boldsymbol{\alpha}^{kT} \tilde{\mathbf{X}}^T \tilde{\mathbf{x}}^k = \boldsymbol{\alpha}^{kT} \mathbf{k}(X, \mathbf{x}^k) \quad (14)$$

where $\mathbf{k}(X, \mathbf{x}) = [k(X_1, \mathbf{x}), \dots, k(X_n, \mathbf{x})]^T$. $k(\cdot, \cdot)$ is the kernel function and $h^k(\cdot)$ is the projection function of the k th view and n is the number of training samples.

By substituting (14) into (6), we find that the loss function of KCVDCA is similar to the one of CVSDCA by replacing \mathbf{U}^p , \mathbf{U}^q , \mathbf{x}_i^p and \mathbf{x}_j^q with $\boldsymbol{\alpha}^p$, $\boldsymbol{\alpha}^q$, $\mathbf{k}(X, \mathbf{x}_i^p)$, and $\mathbf{k}(X, \mathbf{x}_j^q)$, respectively.

Using the reproducing property of the reproduced kernel Hilbert space, $\langle k(\cdot, \mathbf{x}), k(\cdot, \mathbf{y}) \rangle = k(\mathbf{x}, \mathbf{y})$, the regularization terms in the implicit high dimension space can be represented as $\sum_{k=1}^N \boldsymbol{\alpha}^{kT} \mathbf{K} \boldsymbol{\alpha}^k$ and $-\sum_{p=1}^{N-1} \sum_{q=p+1}^N \boldsymbol{\alpha}^{pT} \mathbf{K} \boldsymbol{\alpha}^q$, where \mathbf{K} is the gram matrices defined as $\mathbf{K} = [\mathbf{k}(X, X_1), \mathbf{k}(X, X_2), \dots, \mathbf{k}(X, X_n)]$.

In summary, the optimization problem of KCVDCA is described as follows:

$$\begin{aligned} \min_{\boldsymbol{\alpha}^1, \boldsymbol{\alpha}^2, \dots, \boldsymbol{\alpha}^N} & \sum_{p=1}^{N-1} \sum_{q=p+1}^N \sum_{i=1}^{n^p} \sum_{j=1}^{n^q} \mathbf{W}_{ij}^{p,q} \|\boldsymbol{\alpha}^{pT} \mathbf{k}(X, \mathbf{x}_i^p) - \boldsymbol{\alpha}^{qT} \mathbf{k}(X, \mathbf{x}_j^q)\|_2^2 \\ & + \sum_{p=1}^N \sum_{i=1}^{n^p} \sum_{j=1}^{n^p} \mathbf{W}_{i,j}^{p,p} \|\boldsymbol{\alpha}^{pT} \mathbf{k}(X, \mathbf{x}_i^p) - \boldsymbol{\alpha}^{pT} \mathbf{k}(X, \mathbf{x}_j^p)\|_2^2 \\ & + \text{tr} \left(\lambda \sum_{k=1}^N \boldsymbol{\alpha}^{kT} \mathbf{K} \boldsymbol{\alpha}^k - 2\lambda' \sum_{p=1}^{N-1} \sum_{q=p+1}^N \boldsymbol{\alpha}^{pT} \mathbf{K} \boldsymbol{\alpha}^q \right) \\ \text{s.t. } & \boldsymbol{\alpha}^{kT} \mathbf{M}^k \boldsymbol{\alpha}^k = 1; \quad k = 1, 2, \dots, N \end{aligned} \quad (15)$$

where $\mathbf{M}^k = \mathbf{K}^k \mathbf{K}^{kT} + \lambda \mathbf{K}$ and $\mathbf{K}^k = [\mathbf{k}(X, \mathbf{x}_1^k), \mathbf{k}(X, \mathbf{x}_2^k), \dots, \mathbf{k}(X, \mathbf{x}_{n_k}^k)]$.

E. Closed-Form Solution

To show the solution of the objective function, we take the linear case as an example and the kernel case is similar.

The objective function of the optimization problem (12) can be rewritten as

$$f = \text{tr} \left(\sum_{p=1}^{N-1} \sum_{q=p+1}^N \mathbf{U}^{pT} \mathbf{H}^{p,q} \mathbf{U}^p + \mathbf{U}^{qT} \mathbf{H}^{q,p} \mathbf{U}^q - 2\mathbf{U}^{pT} \mathbf{R}^{p,q} \mathbf{U}^q + \lambda \sum_{k=1}^N \mathbf{U}^{kT} \mathbf{U}^k \right) \quad (16)$$

where $\mathbf{H}^{p,q} = \mathbf{X}^p (\mathbf{D}^{p,q} + \eta \mathbf{D}^{p,p} - \eta \mathbf{W}^{p,p}) \mathbf{X}^{pT}$, where $\mathbf{D}^{p,q}$ is a diagonal matrix whose diagonal entries are defined as $\mathbf{D}_{ii}^{p,q} = \sum_{j=1}^n \mathbf{W}_{ij}^{p,q}$ and $\mathbf{R}^{p,q} = \mathbf{X}^p \mathbf{W}^{p,q} \mathbf{X}^{qT} + \lambda' \mathbf{I}$.

The objective function can be further simplified as

$$f = \text{tr}(\mathbf{U}^T \mathbf{R} \mathbf{U}) \quad (17)$$

where \mathbf{U} is a row-wise concatenated matrix that consists of projection bases of all N views and is defined as

$$\mathbf{U} = [\mathbf{U}^1; \mathbf{U}^2; \dots; \mathbf{U}^N] \in \mathbb{R}^{Nd \times C} \quad (18)$$

and \mathbf{R} is defined as

$$\mathbf{R} = \begin{pmatrix} \mathbf{G}^1 & -\mathbf{R}^{1,2} & \dots & -\mathbf{R}^{1,N} \\ -\mathbf{R}^{2,1} & \mathbf{G}^2 & \dots & -\mathbf{R}^{2,N} \\ \vdots & \vdots & \ddots & \vdots \\ -\mathbf{R}^{N,1} & -\mathbf{R}^{N,2} & \dots & \mathbf{G}^N \end{pmatrix} \quad (19)$$

where $\mathbf{G}^k = \sum_{q \neq k} \mathbf{H}^{k,q} + \lambda \mathbf{I}$.

Note that it is reasonable to relax the constraints $\mathbf{U}^{kT} \mathbf{M}^k \mathbf{U}^k = \mathbf{I}$, $k=1, 2, \dots, N$, to $\sum_{k=1}^N \mathbf{U}^{kT} \mathbf{M}^k \mathbf{U}^k = N\mathbf{I}$, since the relaxed version is sufficient to avoid trivial solution. Therefore, the optimization problem can be modified as

$$\begin{aligned} \min & \text{tr}(\mathbf{U}^T \mathbf{R} \mathbf{U}) \\ \text{s.t.} & \mathbf{U}^T \mathbf{M} \mathbf{U} = N\mathbf{I} \end{aligned} \quad (20)$$

where \mathbf{M} is a block diagonal matrix defined as $\mathbf{M} = \text{diag}(\mathbf{M}^1, \mathbf{M}^2, \dots, \mathbf{M}^N)$.

The optimization problem (20) can be solved by computing c eigenvectors corresponding to the smallest eigenvalues of the following generalized eigendecomposition problem:

$$\mathbf{R} \mathbf{u} = \nu \mathbf{M} \mathbf{u} \quad (21)$$

where ν is the Lagrange multiplier. After getting C eigenvectors $\mathbf{u}_1, \mathbf{u}_2, \dots, \mathbf{u}_C$, the c th transformation basis for the p th view is $\mathbf{u}_c^p = (\delta_p(\mathbf{u}_c) / \|\delta_p(\mathbf{u}_c)\|_{\mathbf{M}})$, where $\delta_p(\cdot)$ means getting the p th subvector and $\|\mathbf{v}\|_{\mathbf{M}} = (\mathbf{v}^T \mathbf{M} \mathbf{v})^{1/2}$.

Since the solution of kernel extension (15) is quite similar to the linear case (12), we do not present its solution in detail. By replacing $\boldsymbol{\alpha}$ with \mathbf{U} , \mathbf{M}^k with \mathbf{M}^k [see (15)], $\mathbf{R}^{p,q}$ with $\mathbf{K}^p \mathbf{D}^{p,q} \mathbf{K}^{qT} + \lambda' \mathbf{K}$, and $\mathbf{H}^{p,q}$ with $\mathbf{K}^p (\mathbf{D}^{p,q} + \eta \mathbf{D}^{p,p} - \eta \mathbf{W}^{p,p}) \mathbf{K}^{pT}$, the solution of the kernel extension can be obtained by solving (21).

F. Properties of the Distance

In this section, we discuss the properties of the proposed asymmetric distance in (2). Strictly speaking, our asymmetric distance is not a conventional metric, and we prove that it satisfies the nonnegativity, symmetry, and triangle inequality properties, but not the coincidence property, and it is actually a pseudometric.

1) *Non-Negativity*: Since d is defined as the L_2 -norm of a vector, it is naturally equal or larger than 0.

2) *Symmetry*: Since

$$\begin{aligned} d(\{\mathbf{x}_i^p, p\}, \{\mathbf{x}_j^q, q\}) &= \|\mathbf{U}^{pT} \mathbf{x}_i^p - \mathbf{U}^{qT} \mathbf{x}_j^q\|_2 \\ &= \|\mathbf{U}^{qT} \mathbf{x}_j^q - \mathbf{U}^{pT} \mathbf{x}_i^p\|_2 \\ &= d(\{\mathbf{x}_j^q, q\}, \{\mathbf{x}_i^p, p\}) \end{aligned} \quad (22)$$

the distance is symmetric. Note that the reason why we call the distance *asymmetric distance* is that the projection bases are different for different camera views.

3) *Triangle Inequality*: Note that

$$\|\mathbf{A} + \mathbf{B}\|_2 \leq \|\mathbf{B}\|_2 + \|\mathbf{A}\|_2 \quad (23)$$

where \mathbf{A} and \mathbf{B} are vectors. By letting $\mathbf{A} = \mathbf{U}^{pT} \mathbf{x}_i^p - \mathbf{U}^{qT} \mathbf{x}_j^q$ and $\mathbf{B} = \mathbf{U}^{rT} \mathbf{x}_k^r - \mathbf{U}^{pT} \mathbf{x}_i^p$, we obtain

$$\begin{aligned} &\|\mathbf{U}^{rT} \mathbf{x}_k^r - \mathbf{U}^{qT} \mathbf{x}_j^q\|_2 \\ &\leq \|\mathbf{U}^{rT} \mathbf{x}_k^r - \mathbf{U}^{pT} \mathbf{x}_i^p\|_2 + \|\mathbf{U}^{pT} \mathbf{x}_i^p - \mathbf{U}^{qT} \mathbf{x}_j^q\|_2. \end{aligned} \quad (24)$$

Thus we have

$$\begin{aligned} &d(\{\mathbf{x}_k^r, r\}, \{\mathbf{x}_j^q, q\}) \\ &\leq d(\{\mathbf{x}_k^r, r\}, \{\mathbf{x}_i^p, p\}) + d(\{\mathbf{x}_i^p, p\}, \{\mathbf{x}_j^q, q\}). \end{aligned} \quad (25)$$

4) *Coincidence*: It is noted that $d(\{\mathbf{x}^p, p\}, \{\mathbf{x}^q, q\}) = 0$ holds if and only if $\mathbf{U}^{pT} \mathbf{x}^p = \mathbf{U}^{qT} \mathbf{x}^q$, which means $[\mathbf{U}^p; -\mathbf{U}^q]^T [\mathbf{x}^p; \mathbf{x}^q] = 0$, which could be an underdetermined problem. Therefore, there exist an infinite number of inputs $\{\mathbf{x}^p, p\}, \{\mathbf{x}^q, q\}$ that satisfy $d(\{\mathbf{x}^p, p\}, \{\mathbf{x}^q, q\}) = 0$. That means $d(\{\mathbf{x}^p, p\}, \{\mathbf{x}^q, q\}) = 0$ does not always imply $\{\mathbf{x}^p, p\} = \{\mathbf{x}^q, q\}$. However, fortunately, one still has $d(\{\mathbf{x}^p, p\}, \{\mathbf{x}^p, p\}) = \|\mathbf{U}^{pT} \mathbf{x}^p - \mathbf{U}^{pT} \mathbf{x}^p\|_2 = 0$. Therefore, the coincidence property does not strictly holds, and our distance is in fact a pseudometric. However, this does not hurt the model for practical use. It is not practical for visual surveillance to have the constraint that $d(\{\mathbf{x}^p, p\}, \{\mathbf{x}^q, q\}) = 0$ only when $\{\mathbf{x}^p, p\} = \{\mathbf{x}^q, q\}$. In visual surveillance, it is rare to have the same appearance representation for the same person at different camera views due to the existence of view changes and lighting changes. Hence, it is more practical to say two images are from the same person if they are having the same representation in the transformed space (i.e., $\mathbf{U}^{pT} \mathbf{x}^p = \mathbf{U}^{qT} \mathbf{x}^q$), while ensuring the optimization that two images of different people have different representations in that space.

IV. EXPERIMENTAL RESULTS

A. Data Sets and Settings

1) *Data Sets*: The evaluation of the proposed method is carried out on six challenging data sets: SYSU [1],

PRID450S [38], VIPeR [48], CUHK01 [49], CAVIAR4REID [50], and RAiD [51]. A significant feature discrepancy can be observed in all the six data sets. PRID450S contains 450 image pairs recorded from two different but static surveillance cameras. In this set, masks generated both automatically and manually were provided to define the foreground regions of interest. VIPeR contains 632 pedestrian image pairs captured outdoor with varying viewpoints and illumination conditions. Each image is scaled to 128×48 pixels. CUHK01 contains 971 pedestrians from two disjoint camera views. Each pedestrian has two samples per camera view. SYSU contains totally 48892 images of 502 pedestrians captured by two cameras. CAVIAR4REID contains 72 pedestrians of which 50 are viewed in disjoint camera views and 22 are not. Totally, 1220 images are included in the data set. RAiD contains four camera views with two indoor and two outdoor. Forty-three pedestrians are included in the data set, resulting in 6920 images. Among the 43 pedestrians, 41 of them appeared in all four camera pairs. Illumination and pose greatly change across the different camera views. Although there are other data sets publically available, such as iLIDS [52] and ETHZ [53], we do not conduct experiments on them because our method utilize the camera view label information and those data sets do not provide it.

2) *Features*: To validate the effectiveness of the proposed method, we extracted only low-level color and texture features in the following experiments. Specifically, we equally partitioned each image into 18 nonoverlapped horizontal stripes. For each stripe, RGB, HSV, YCbCr, Lab, and YIQ color features as well as 16 Gabor texture features were extracted. For each feature channel, a 16-bin histogram was extracted. In order to balance the weight of each type of feature, we normalized all histograms by L_1 -norm. All histograms were concatenated together to form a single vector. Since PRID450S provides automatically generated foreground masks, our features were extracted from the foreground; for other data sets, our features were extracted from the whole image.

The extracted feature contains rich information since it was extracted from dense horizon stripe, including various color space and texture features. However, it is sensitive to illumination or viewpoint changes, so features of different views could suffer great discrepancy.

3) *Experimental Protocol*: All data sets were evaluated with the same training protocol: each time half of the pedestrians were selected randomly to form the training set, and the remaining pedestrian images were used to form a testing set. Since there are 22 pedestrians whose images were only captured in a single view in CAVIAR4REID, we did not select them for experiments and only used the rest 50 pedestrians for evaluation. On RAiD, we followed the experimental protocol in [24], i.e., we used camera pairs 1-3, 1-4, and 3-4 for evaluation [denoted by RAiD(1-3), RAiD(1-4), and RAiD(3-4)], and each pedestrian has ten images for each view in the multishot experiment. On SYSU, we randomly pick three images of each pedestrian in each view for evaluation.

The performance was evaluated by both single-shot protocol, i.e., only one image each person was registered in

the gallery set, and multishot protocol, i.e., at least two images each person were registered. For metric learning methods, when comparing the distance between a probe person and a gallery person in the gallery set, we calculate the average of the learned distance between a probe image and each of the registered images of that gallery person.

The performance was evaluated with both closed-set protocol and open-set protocol. The cumulative matching characteristic (CMC) curve was used for evaluating the closed-set performance. A rank k matching rate in the CMC curve indicates the percentage of the probe image with correct matches found in the top k rank against the p gallery images. In practice, a high rank-1 matching rate is critical and the top k matching rank matching rate with a small k value is also important since the top matching images can be verified by human [8].

To simulate the open-set situation, we also randomly discarded 20% of the gallery images, and thus some of the people in the probe set are not known from the gallery set. In order to quantify how well a true target have been verified and how bad a false target have mistakenly passed through the verification, we followed [35] to use the true target rate (TTR) and false target rate (FTR) to evaluate the performance. TTR and FTR are defined as

$$\begin{aligned} \text{TTR} &= \frac{n_{\text{TT}}}{n_T} \\ \text{FTR} &= \frac{n_{\text{NT}}}{n_N} \end{aligned} \quad (26)$$

where n_T indicates the number of query target images from target people, n_{TT} indicates the number of query images that are verified as one of the target people, n_{NT} indicates the number of nontarget images from nontarget people, and n_N indicates the number of query nontarget images that are verified as one of the target people.

4) *Methods for Comparison*: We first compared our methods with symmetric distance learning methods including Relative Distance Comparison (RDC) [8], LFDA [9], KISSME [17], Kernel Local Fisher Discriminant Analysis (KLFDA) [28], and regularized kernel PCCA (rKPCCA) [28]. We also evaluated the rCCA [54] and CMML [45], which provide view-specific mappings. In our comparison, all methods used the same features, and thus the performance difference is only due to the different processing on the extracted features.

We also discuss the comparison of our methods with the state-of-the-art methods in Section IV-C, which is on the system-level comparison in order to compare with the state-of-the-art.

5) *Parameter*: In the following experiments, we set both η and γ to 0.1 for both CVDCA and KCVDC. In order to balance the scale of the objective function and the feature consistency regularization term, λ' was set to 10^{-3} for CVDCA and 0.3 for KCVDC. All parameters were fixed for all data sets, and we will discuss those parameters in Section IV-D.

B. Comparison With the Distance/Subspace Learning Methods

1) *Closed-Set Evaluation*: We first discuss the closed-set situation where people in the probe set are represented in

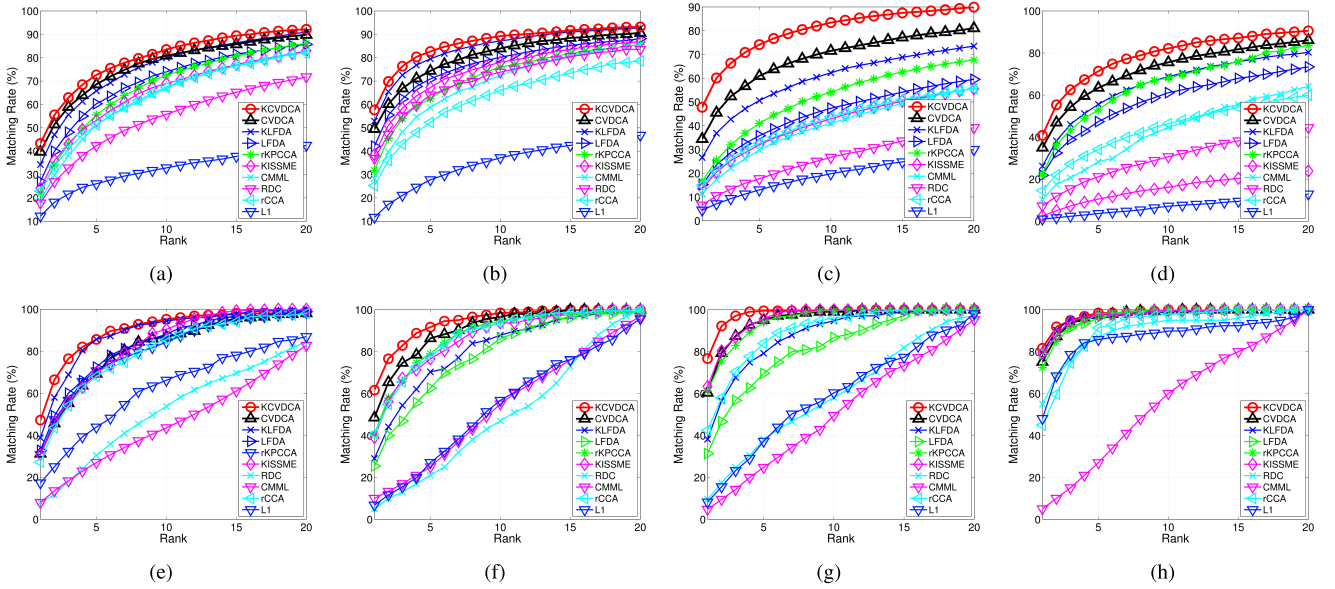


Fig. 4. CMC curves on VIPeR, PRID450S, CUHK01, SYSU, CAVIAR4REID, and RAiD(1-3), RAiD(1-4), and RAiD(3-4). (a) VIPeR. (b) PRID450S. (c) CUHK01. (d) SYSU. (e) CAVIAR4REID. (f) RAiD(1-3). (g) RAiD(1-4). (h) RAiD(3-4). Best viewed in color.

TABLE I

TOP-RANKED MATCHING RATE (%) ON VIPeR, PRID450S, CUHK01, SYSU, CAVIAR4REID, RAiD(1-3), RAiD(1-4), AND RAiD(3-4)

dataset	VIPeR				PRID450S				CUHK01				SYSU			
	rank	1	5	10	20	1	5	10	20	1	5	10	20	1	5	10
KCVDCA	43.29	72.66	83.51	92.18	57.60	82.67	89.24	93.20	47.80	74.16	83.44	89.92	40.84	71.35	82.19	90.56
CVDCA	39.72	68.58	80.89	89.78	49.47	74.36	83.96	90.62	34.14	60.95	71.52	81.05	34.98	63.43	75.58	86.10
KLFDA [28]	34.27	65.82	79.94	90.92	52.84	79.51	87.20	92.80	26.62	50.63	62.28	73.50	28.69	58.21	70.96	82.39
LFDA [9]	27.03	60.28	73.99	85.70	42.09	70.93	80.18	88.18	15.22	35.80	47.37	59.52	26.22	55.62	68.80	80.32
rKPCCA [6]	22.28	55.47	72.41	86.04	31.82	62.40	76.00	85.73	16.68	41.00	54.11	67.73	22.31	52.99	68.13	83.67
KISSME [17]	24.21	53.10	68.99	82.97	38.49	67.20	78.09	86.89	13.53	31.99	42.89	55.56	16.85	39.84	54.66	68.96
RDC [8]	17.75	42.34	55.73	71.77	36.89	64.00	73.78	83.56	6.56	17.68	26.69	39.16	7.21	21.16	30.68	44.46
CMML [45]	18.77	51.17	66.77	82.31	28.27	58.71	72.40	85.60	11.45	29.72	40.98	56.03	10.36	28.29	44.62	64.14
rCCA [54]	22.94	51.23	67.44	82.09	25.24	52.31	66.13	78.62	14.90	32.59	43.77	55.53	14.58	34.14	46.37	59.96
L_1	12.15	26.01	32.82	42.47	11.64	27.73	37.16	46.76	4.45	12.97	19.80	29.94	1.00	3.67	7.13	12.91
dataset	CAVIAR4REID				RAiD(1-3)				RAiD(1-4)				RAiD(3-4)			
rank	1	5	10	20	1	5	10	20	1	5	10	20	1	5	10	20
KCVDCA	47.20	85.60	95.20	98.40	61.64	91.69	98.50	100.00	76.69	99.50	99.50	100.00	81.63	98.45	100.00	100.00
CVDCA	31.20	69.20	86.80	98.00	48.50	86.33	96.57	100.00	60.36	95.12	99.00	100.00	75.05	97.45	99.47	100.00
KLFDA [28]	38.80	85.60	94.40	99.20	29.02	70.36	87.83	100.00	38.21	79.21	94.64	100.00	79.58	96.45	99.00	100.00
LFDA [9]	30.00	67.60	85.20	98.40	25.40	62.57	86.29	99.02	31.38	69.62	86.81	100.00	81.37	98.00	99.50	100.00
rKPCCA [6]	30.77	73.08	80.77	100.00	40.57	79.00	94.62	99.02	61.24	94.07	99.52	100.00	72.37	98.00	100.00	100.00
KISSME [17]	30.77	70.00	90.38	100.00	39.02	76.60	93.71	100.00	63.33	95.64	100.00	100.00	79.29	97.50	99.50	100.00
RDC [8]	8.00	30.40	53.76	84.64	5.00	21.00	47.00	100.00	9.52	38.10	58.10	96.83	55.00	87.00	95.00	100.00
CMML [45]	8.00	27.00	43.55	82.74	10.00	25.00	55.00	96.67	4.76	24.76	49.52	95.24	5.00	27.00	60.00	100.00
rCCA [54]	27.20	68.00	85.60	98.00	40.76	77.62	93.60	100.00	42.50	84.00	96.14	100.00	44.95	91.34	97.97	100.00
L_1	17.31	43.85	66.15	86.92	6.76	27.07	56.71	95.62	8.21	37.21	60.33	98.05	48.05	85.76	89.84	100.00

the gallery set, which is a conventional person reidentification test. Fig. 4 shows the CMC curves on VIPeR, PRID450S, CUHK01, SYSU, CAVIAR4REID, and RAiD, respectively, and Table I shows the top-ranked matching rate on these data sets.

(K)CVDCA Versus Baseline: We first compared our methods with the L_1 baseline. Table I shows that L_1 does not perform well in all the six data sets. Note that the features we used consist of low-level color and texture features, which are sensitive to the environmental changes across views. Since L_1 is a nonlearning distance measure, it is not robust to those changes. Our methods learn asymmetric distance for better

measuring the distance of pedestrian images across camera views, and thus they achieve a significant improvement.

(K)CVDCA Versus Symmetric Distance Learning: Symmetric distance learning methods, including (K)LFDA, rKPCCA, KISSME, Large Margin Nearest Neighbor metric learning (LMNN), and RDC, are most relevant to our methods. The major difference is that symmetric distance learning methods map the original features to a new space with a unitary mapping, while our methods allow different mappings for different camera views. As such, symmetric distance learning assumes that the features used for distance measurements can be both discriminative and invariant to environmental

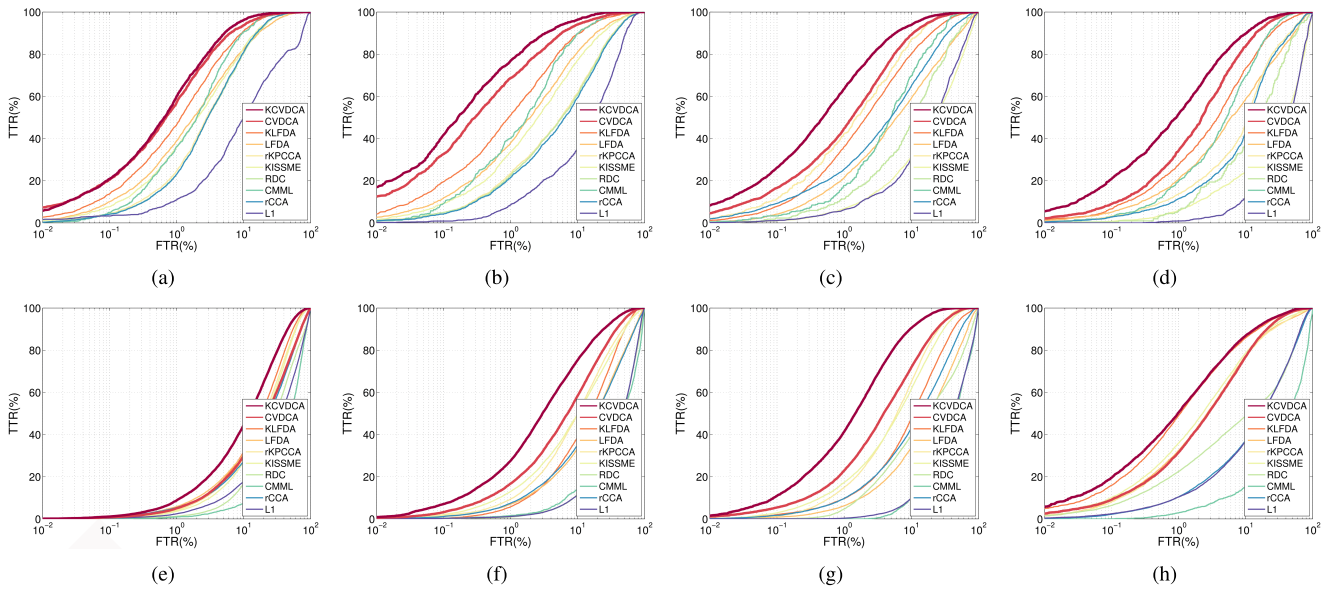


Fig. 5. TTR–FTR curves on VIPeR, PRID450S, CUHK01, SYSU, CAVIAR4REID, RAiD(1-3), RAiD(1-4), and RAiD(3-4). (a) VIPeR. (b) PRID450S. (c) CUHK01. (d) SYSU. (e) CAVIAR4REID. (f) RAiD(1-3). (g) RAiD(1-4). (h) RAiD(3-4). Better viewed in color.

changes, while asymmetric distance learning does not hold such a restricted assumption. Hence, our methods weaken the assumption of distance learning previously used in person reidentification and achieve notable improvement compared with symmetric distance learning methods. Among those symmetric distance learning methods, KLFDA/LFDA achieves a relatively good performance. KCVDCA achieves 9.02%, 4.76%, 21.18%, 12.15%, 9.00%, 32.64%, 38.48%, and 2.05% improvements over KLFDA at rank 1 on VIPeR, PRID450S, CUHK01, SYSU, CAVIAR4REID, RAiD(1-3), RAiD(1-4), and RAiD(3-4), respectively, and for linear case, the difference of rank-1 between CVDCA and LFDA is 12.69%, 7.38%, 18.94%, 8.76%, 1.20%, 23.10%, 28.98%, and -6.32% on those data sets, respectively. The improvement is particularly notable on SYSU, CUHK01, RAiD(1-3), and RAiD(1-4). The illumination changes of these data sets are extremely large [see Fig. 2(a), (f), and (g)], and the difference in features of two images is caused more by the lighting change than that by the pedestrian identities. Since our methods learn asymmetric distance, i.e., view-specific mapping is used for each view, the influence of lighting change is suppressed and the distance model for matching is more relevant to pedestrian identities. A later evaluation in Section IV-D1 further shows that the performance of our methods would drop notably when they degrade to symmetric distance models. Also note that in RAiD(3-4), KCVDCA performs only slightly better than KLFDA. It is because in the RAiD data set, cameras 3 and 4 are both outdoor cameras, and the environmental condition such as illumination does not change much [see Fig. 2(h)]. Thus, our methods do not show a significant advantage in this setting. For indoor–outdoor settings like RAiD(1-3) and RAiD(1-4), our methods performs much better.

(K)CVDCA Versus Multimodal Learning: Multimodal learning methods including CMML and rCCA were also evaluated in our experiments. They are related to our model since they

and ours all can learn view-specific feature transformations. However, those methods deal with the problem when features of different views are heterogeneous, while for the person reidentification problem we discuss in this paper that the features of person images under different camera views are not heterogeneous but related. Nevertheless, these methods do not perform well on person reidentification. In contrast, our methods model the relation between view-specific feature transformations with the feature consistency regularization and thus perform much better.

2) *Open-Set Evaluation*: In addition to the closed-set performance evaluation, we also report the open-set performance as Fig. 5. Note that in the open-set setting, some identities in the probe set are not known in the gallery set, and our objective is to verify whether a query image comes from the people in the gallery set. The TTR versus FTR curve defined by (26) was used for evaluation. Clearly, our method also achieves the best performance among all methods in comparison. Specifically, when $FTR = 10\%$, the TTRs of KCVDCA are 96.21%, 96.33%, 93.93%, 89.05%, 44.52%, 75.32%, 90.55%, and 86.93% on VIPeR, PRID450S, CUHK, SYSU, CAVIAR4REID, RAiD(1-3), RAiD(1-4), and RAiD(3-4), respectively, while for KLFDA, they are 90.99%, 89.67%, 80.21%, 73.38%, 31.83%, 38.88%, 47.75%, and 85.84%, respectively.

C. Comparison With the State-of-the-Art Methods

The proposed method is compared with the state-of-the-art methods using the same evaluation protocols. Tables II–VII show the top matching rate on the VIPeR, PRID450S, CUHK01, RAiD and CAVIAR4REID data sets, and Fig. 6 shows the CMC curves. Note that SYSU is a newly released data set and to the best of our knowledge, there is no supervised method conducted on this data set and therefore it is not used in this section.

TABLE II
TOP-RANKED MATCHING RATE (%) ON RAiD(1-3), RAiD(1-4), AND RAiD(3-4)

camera pair	pair 1-3				pair 1-4				pair 3-4			
	rank	1	5	10	20	1	5	10	20	1	5	10
KCVDCA	61.64	91.69	98.50	100.00	76.69	99.50	99.50	100.00	81.63	98.45	100.00	100.00
NCR on FT [51]	67.00	83.00	93.00	100.00	68.00	86.00	99.00	100.00	79.00	93.00	98.00	100.00
FW [24]	46.17	82.86	94.76	99.25	53.81	90.00	98.10	100.00	55.67	90.87	99.12	100.00
WACN [56]	14.89	55.46	78.89	99.28	22.40	64.07	89.48	99.88	38.07	75.62	93.07	99.50
SDALF [57]	12.19	44.99	73.95	99.07	16.99	57.22	83.17	99.60	33.99	72.36	90.07	99.77
ICT [58]	29.52	70.95	91.43	99.05	37.14	79.52	96.19	100.00	40.95	84.76	96.67	100.00
ISR [30]	5.88	24.83	51.71	97.62	8.81	32.40	51.55	98.57	58.79	86.92	92.45	95.25

TABLE III

TOP-RANKED MATCHING RATE (%) ON CAVIAR4REID ($N = 5$)

rank	1	5	10	20
KCVDCA	36.80	78.80	92.40	99.20
FW [24]	33.20	78.50	94.10	100.00
LFDA [9]	36.19	66.15	88.56	98.41
ISR [30]	14.40	47.60	69.60	94.40

TABLE IV

TOP-RANKED MATCHING RATE (%) ON CAVIAR4REID ($N = 10$)

rank	1	5	10	20
KCVDCA	45.60	86.00	95.60	99.60
FW [24]	41.90	86.50	96.70	100.00
ICT [58]	26.80	70.40	90.00	99.60
ISR [30]	18.40	50.00	71.20	95.60

TABLE V

TOP-RANKED MATCHING RATE (%) ON VIPeR COMPARED WITH THE STATE-OF-THE-ART METHODS

rank	1	5	10	20
KCVDCA(Fusion)	47.78	76.33	86.33	94.02
MLF+LADF [2]	43.39	73.04	84.87	93.70
MLF [2]	29.11	52.34	65.95	79.87
Ref-Reid [40]	33.29	63.54	78.35	88.48
SalMatch [22]	30.16	52.31	65.54	79.15
LADF [18]	29.34	61.04	75.98	88.10
LFDA [9]	24.18	52.00	67.12	82.00
RDC [8]	15.66	38.42	53.86	70.09

On VIPeR, MLF + LADF [2] combines the result of Mid-Level Filter (MLF) and LADF. For fair comparison, we trained the proposed KCVDCA method using both of our low-level features and high-level texture features [55] used by LADF [18], and then simply summed up the score as did in MLF+LADF [2]. Fig. 6(a) shows that our method achieves the best performance on this data set. We have compared our algorithm with the SCNCD [4], LMNN [5], Information Theoretic Metric Learning (ITML) [7], KISSME [17], Efficient Imposter-based Metric Learning [19], and Large Margin Nearest Neighbor with Rejection [20] on PRID450S, and compared our algorithm with MLF [2], enriched Saliency Distance Comparison [3], LMNN [5], ITML [7], SalMatch [22], and Ref-Reid [39] on CUHK01. Fig. 6(b) and (c) shows that our approach outperforms other approaches by a large margin.

On the RAiD data set, we have compared our algorithm with the recently proposed LFDA [9], FW [24], Network Consistent Re-identification [51],

TABLE VI

TOP-RANKED MATCHING RATE (%) ON PRID450S COMPARED WITH THE STATE-OF-THE-ART METHODS

rank	1	5	10	20
KCVDCA	57.60	82.67	89.24	93.20
SCNCD(imgF) [4]	42.44	69.22	79.56	88.44
KISSME [17]	33.47	59.82	70.84	79.47
EIML [19]	34.71	57.73	67.91	77.33
LMNN [5]	28.98	55.29	67.64	78.36
LMNN-R [20]	21.96	46.22	58.53	71.20
ITML [7]	24.27	47.82	58.67	70.89

TABLE VII

TOP-RANKED MATCHING RATE (%) ON CUHK01 COMPARED WITH THE STATE-OF-THE-ART METHODS

rank	1	5	10	20
KCVDCA	47.80	74.16	83.44	89.92
MLF [2]	34.30	55.06	64.96	74.94
Ref-Reid [40]	31.10	57.10	68.55	79.18
ITML [7]	15.98	35.22	45.60	59.81
LMNN [5]	13.45	31.33	42.25	54.11
SalMatch [22]	28.45	45.85	55.67	67.95
eSDC(KNN) [3]	19.67	32.72	40.29	50.58

Wide Area Camera Network [56], Symmetry-Driven Accumulation of Local Features [57], Implicit Camera Transfer [58], and Interactive Sparse Ranking (ISR) [30]. Fig. 6(d)–(f) and Table II show that our method could achieve the state-of-the-art performance on all the three camera pairs.

On CAVIAR4REID, our approach achieves overall better results. In particular, FW [24] is comparable with our approach, as observed from Fig. 6(g) and (h). In comparison with ISR [30], the proposed method achieves clearly better results. Note that the testing protocol used by ISR in [30] is different from ours, i.e., the gallery and probe images are strictly from different camera views in our setting. The experiment shows that ISR does not perform well when matching person images from disjoint/different camera views probably because the gallery images may not be able to reconstruct the probe one very well.

D. Discussion

1) *Effectiveness of Cross-View Consistency Regularization:* As discussed in III-C, the cross-view consistency regularization is critical to avoid learning arbitrarily different projections for different views. Fig. 7(a) shows the effectiveness of this regularization on PRID450S, for example, and similar conclusion can be drawn on the others. Note that if the penalty

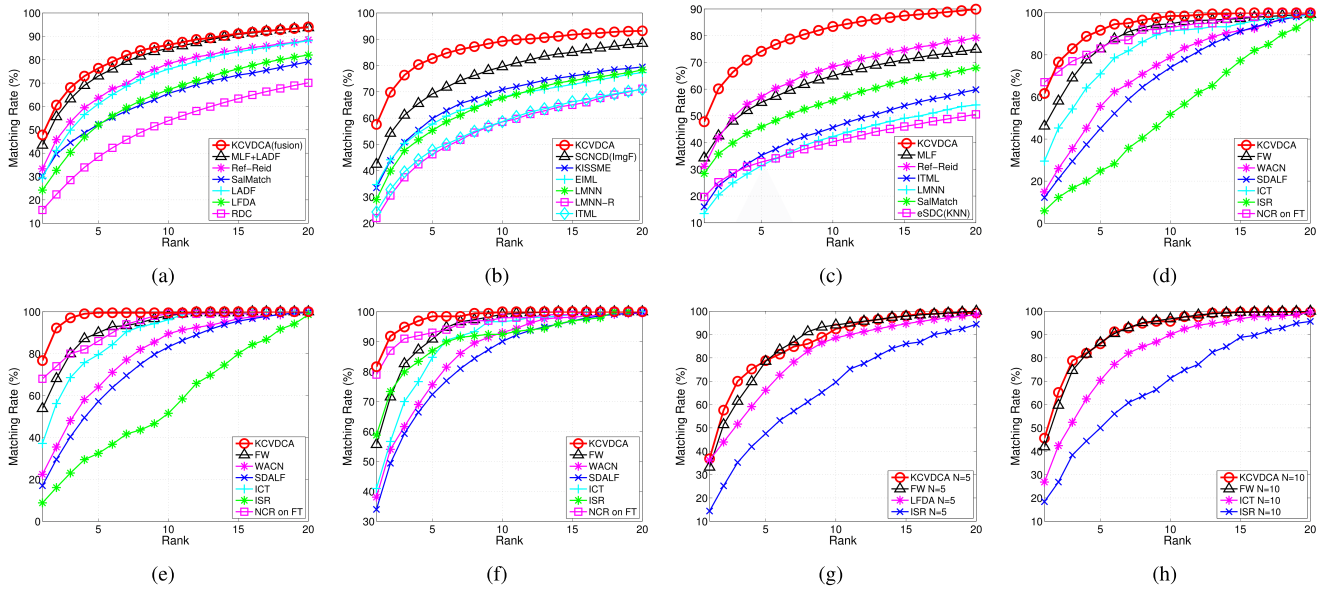


Fig. 6. Comparison with the state-of-the-art performance on VIPeR, PRID450S, CUHK01, CAVIAR4REID, and RAiD. (a) VIPeR. (b) PRID450S. (c) CUHK01. (d)–(f) Experiments conducted on camera pairs 1-3, 1-4, and 3-4 of RAiD, respectively. (g) and (h) Multishot experiments conducted on CAVIAR4REID with five and ten images per pedestrian, respectively. Best viewed in color.

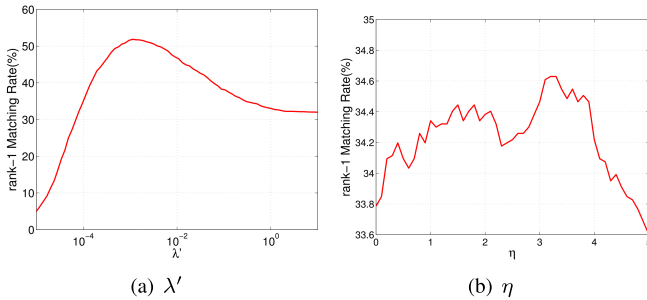


Fig. 7. Parameter analysis of CVDCA. (a) Parameter of cross-view consistency regularization. (b) Parameter of intra-view modeling.

term λ' is infinitely small, the effect of this regularization vanishes and the rank-1 matching rate is less than 10%; as λ' increases, the rank-1 matching rate increases simultaneously until it reaches the maximum, which is larger than 50%. If the penalty term is set too large, it then tends to ignore the feature discrepancy across views and thus the performance drops. Note that when this penalty term is infinitely large, the view-specific mappings would be the same and asymmetric distance learning degrades to symmetric distance learning. Hence, the experimental results validate our analysis that a proper cross-view consistency regularization is critical for asymmetric distance learning.

2) *Effectiveness of Intra-View Modeling*: Our model (12) consists of both cross-view and intra-view modeling. We argue that the cross-view modeling plays a major role for the person reidentification problem and the intra-view modeling may have relative limited effectiveness to the cross-view matching problem. Fig. 7(b) shows the weight of intra-view modeling η versus the rank-1 matching rate on the CUHK01 data set and a similar conclusion can be drawn on the others. Note that when $\eta = 0$, the intra-view modeling part is removed and only the cross-view modeling contributes to the performance, and

the rank-1 matching rate is 33.8%. Tuning η does boost the performance and the maximum rank-1 matching rate is 34.6%, which indicates that the intra-view modeling is useful, albeit limited.

Note that the widely used testing protocol for person reidentification is to match pedestrians across camera views, while the intra-view matching is not the concern. Hence, it is reasonable that the cross-view modeling plays more important part in the modeling. The intra-view modeling to an extent is related to the matching, and thus incorporating it to the model could help tackling the cross-view matching problem.

3) *Brief Analysis of the Extracted Features*: Throughout the experimental section, we have shown that our asymmetric distance performs better than the symmetric ones. Our explanation is that using different mappings for different camera views, we can extract more discriminative features, even if those features are divergent for each view. On the contrary, using a unitary mapping for all views would have to discard some of the discriminative features if they are divergent.

Taking PRID450S as an example, we give an analysis on the difference in features extracted by the asymmetric distance learning method (CVDCA) and the symmetric distance learning method (LFDA). We semantically divided the features into color features (including RGB, HSV, YCbCr, Lab, and YIQ features) and texture features (the Gabor features). As shown in Fig. 8, color features are more discriminative than texture features, as using color features results in better performance than using texture features. However, as shown in Fig. 3, color features on this data set are very different across the two camera views, while in Fig. 9, we can observe that texture features are much more consistent across the two views.

We trained CVDCA and LFDA with the color + texture features and obtained the projection bases U^a and U^b (for LFDA, $U^a = U^b$). Then we calculated the energy for

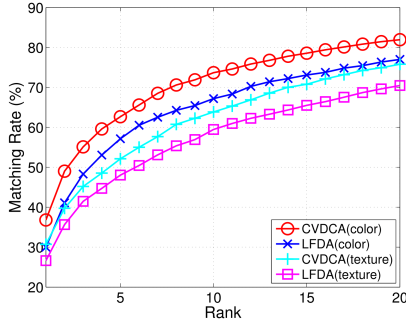


Fig. 8. Performance using different feature types.

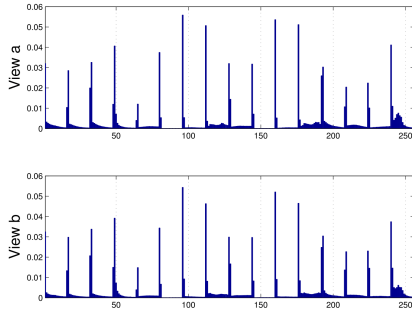
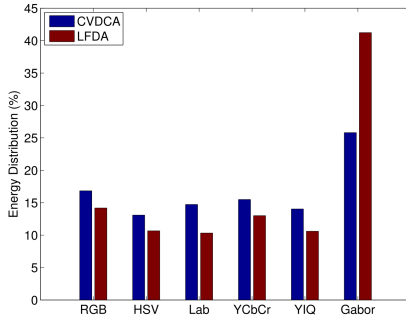
Fig. 9. Illustration of Gabor features of PRID450S. Similar to Fig. 3, the first row shows the Gabor feature distributions of $(1/n_p^{a,b}) \sum_i x_i^a$ and the second row shows those of $(1/n_p^{a,b}) \sum_j x_j^b$.

Fig. 10. Energy distribution of different feature types. Energy is defined as in (27). We compare the percentage of energy of different feature types between CVDCA and LFDA.

each type of features as follows:

$$E(f) = \sum_k \sum_{j \in B_f} (U^a(k, j)^2 + U^b(k, j)^2) \quad (27)$$

where $f \in \{\text{RGB, HSV, YCbCr, Lab, YIQ, Gabor}\}$ indicates the set of feature types, B_f is the set of indices of feature type f , and $U^a(k, j)$ is the k th column and j th row of matrix U^a . Fig. 10 shows the energy distribution of different feature types of CVDCA and LFDA. It shows that CVDCA allots more energy to the color features, while LFDA allots more to the texture features. Recall that color features are more discriminative but divergent, while texture features are less discriminative but more divergent. Therefore, we conclude that more color features, which is shown to be more discriminative, are preserved by our approach.

V. CONCLUSION

In this paper, we address the feature discrepancy problem across nonoverlapping camera views for person reidentification. A CVDCA method, which forms an asymmetric distance model for matching person images between disjoint camera views by learning view-specific mappings, is proposed to overcome this problem. To model the correlation nature of feature transformations of different views, a cross-view consistency regularization is introduced in our model. The experimental results demonstrate that: 1) the asymmetric distance model performs notably better than the symmetric ones and 2) the influence of feature discrepancy can be effectively alleviated by view-specific modeling.

In this work, we use Euclidean distance as the measure of the discrepancy of different mappings in the cross-view consistency regularization, which implicitly assumes Gaussian distribution for the projection matrices. However, how to relax such an assumption remains a future issue to investigate. In our future works, we would like to investigate other examples of the Bregman distance, which could work better for more general distributions in the exponential families.

APPENDIX

PROBABILISTIC INTERPRETATION

In the following, we will give a probabilistic interpretation of the cross-view consistency regularization. The cross-view consistent regularization can be viewed as prior knowledge of the projection matrices.

The term $\|U^p T x_i^p - U^q T x_j^q\|_2^2$ can be rewritten as

$$\begin{aligned} & \|U^p T x_i^p - U^q T x_j^q\|_2^2 \\ &= [x_i^p; x_j^q]^T [U^p; -U^q] [U^p; -U^q]^T [x_i^p; x_j^q] \\ &= \text{tr}([x_i^p; x_j^q][x_i^p; x_j^q]^T [U^p; -U^q][U^p; -U^q]^T) \\ &= \text{vec}([x_i^p; x_j^q][x_i^p; x_j^q]^T) \text{vec}([U^p; -U^q][U^p; -U^q]^T), \end{aligned} \quad (28)$$

where $[A; B]$ means concatenating vector/matrix A and B in column, $\text{tr}(A)$ is the trace of matrix A , and $\text{vec}(A)$ denotes vectorizing matrix A . Therefore, (7) is related to a specific distribution in the exponential family

$$p_{\text{cross}}(D|U^p, p = 1, 2, \dots, N) = \kappa \prod_{p=1}^{N-1} \prod_{q=p+1}^N \prod_{i=1}^{n^p} \prod_{j=1}^{n^q} \exp(-\mathbf{W}_{ij}^{p,q} \mathbf{u}(x_i^p, x_j^q)^T \boldsymbol{\eta}(U^p, U^q)), \quad (29)$$

where D is the notion of a dataset, $\mathbf{u}(x_i^p, x_j^q) = \text{vec}([x_i^p; x_j^q][x_i^p; x_j^q]^T)$, $\boldsymbol{\eta}(U^p, U^q) = \text{vec}([U^p; -U^q][U^p; -U^q]^T)$, and κ is a normalization term.

Similarly, (8) is related to another distribution in an exponential family

$$p_{\text{intra}}(D|U^p, p = 1, 2, \dots, N) = \kappa \prod_{p=1}^N \prod_{i=1}^{n^p} \prod_{j=1}^{n^p} \exp(-\mathbf{W}_{ij}^{p,p} \mathbf{u}(x_i^p, x_j^p)^T \boldsymbol{\eta}(U^p, U^p)). \quad (30)$$

Therefore, the objective function of Eq. (10) can be rewritten as

$$\max_{U^p, p=1,2,\dots,N} p_{\text{cross}} * p_{\text{intra}}, \quad (31)$$

which can be interpreted as maximizing the likelihood probability.

With this probabilistic interpretation, the regularization can be viewed as prior knowledge of U^p and U^q , which is $p_{prior} = \prod_{p=1}^{N-1} \prod_{q=p+1}^N \exp(-d_{\mathcal{F}}(U^p, U^q))$. Integrating this prior knowledge, the optimization problem turns to

$$\max_{U^p, p=1,2,\dots,N} P_{cross} * P_{intra} * P_{prior}. \quad (32)$$

Note that different Bregman distance corresponds to different prior distribution. Without further knowledge of the projection matrices, it is more reasonable to assume that the difference of two projection matrices follows the Gaussian distribution, which means $p_{prior} = \kappa \prod_{p=1}^{N-1} \prod_{q=p+1}^N \exp(-\lambda \|U^p - U^q\|_2^2)$. Note that (12) can be obtained by imposing $-\log$ operator to (32). In this way, the CVDCA has an probabilistic interpretation with a Gaussian prior assumption. Our empirical results show that this Gaussian assumption results in satisfying performance, and it also makes the optimization problem easy to solve.

ACKNOWLEDGMENT

The authors would like to thank the anonymous reviewers for providing the constructive advice on the revision of this paper.

REFERENCES

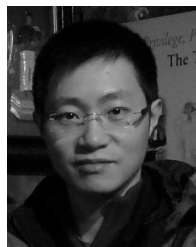
- [1] C.-C. Guo, S.-Z. Chen, J.-H. Lai, X.-J. Hu, and S.-C. Shi, "Multi-shot person re-identification with automatic ambiguity inference and removal," in *Proc. 22nd ICPR*, 2014, pp. 3540–3545.
- [2] R. Zhao, W. Ouyang, and X. Wang, "Learning mid-level filters for person re-identification," in *Proc. IEEE Conf. CVPR*, Jun. 2014, pp. 144–151.
- [3] R. Zhao, W. Ouyang, and X. Wang, "Unsupervised salience learning for person re-identification," in *Proc. IEEE Conf. CVPR*, Jun. 2013, pp. 3586–3593.
- [4] Y. Yang, J. Yang, J. Yan, S. Liao, D. Yi, and S. Z. Li, "Salient color names for person re-identification," in *Proc. 13th ECCV*, 2014, pp. 536–551.
- [5] K. Q. Weinberger, J. Blitzer, and L. K. Saul, "Distance metric learning for large margin nearest neighbor classification," in *Proc. NIPS*, 2006, pp. 1473–1480.
- [6] A. Mignon and F. Jurie, "PCCA: A new approach for distance learning from sparse pairwise constraints," in *Proc. IEEE Conf. CVPR*, Jun. 2012, pp. 2666–2672.
- [7] J. V. Davis, B. Kulis, P. Jain, S. Sra, and I. S. Dhillon, "Information-theoretic metric learning," in *Proc. 24th ICML*, 2007, pp. 209–216.
- [8] W.-S. Zheng, S. Gong, and T. Xiang, "Reidentification by relative distance comparison," *IEEE Trans. Pattern Anal. Mach. Intell.*, vol. 35, no. 3, pp. 653–668, Mar. 2013.
- [9] S. Pedagadi, J. Orwell, S. Velastin, and B. Boghossian, "Local Fisher discriminant analysis for pedestrian re-identification," in *Proc. IEEE Conf. CVPR*, Jun. 2013, pp. 3318–3325.
- [10] F. Porikli, "Inter-camera color calibration by correlation model function," in *Proc. ICIP*, Sep. 2003, pp. II-133–II-136.
- [11] B. Prosser, S. Gong, and T. Xiang, "Multi-camera matching using bi-directional cumulative brightness transfer functions," in *Proc. BMVC*, 2008, pp. 64.1–64.10.
- [12] C. Siebler, K. Bernardin, and R. Stiefelwagen, "Adaptive color transformation for person re-identification in camera networks," in *Proc. 4th ICSDC*, 2010, pp. 199–205.
- [13] C. Liu, S. Gong, C. C. Loy, and X. Lin, "Person re-identification: What features are important?" in *Proc. ECCV Workshops*, 2012, pp. 391–401.
- [14] E. P. Xing, M. I. Jordan, S. J. Russell, and A. Y. Ng, "Distance metric learning with application to clustering with side-information," in *Proc. NIPS*, 2002, pp. 505–512.
- [15] J. Goldberger, G. E. Hinton, S. T. Roweis, and R. Salakhutdinov, "Neighbourhood components analysis," in *Proc. NIPS*, 2004, pp. 513–520.
- [16] M. Sugiyama, "Dimensionality reduction of multimodal labeled data by local Fisher discriminant analysis," *J. Mach. Learn. Res.*, vol. 8, pp. 1027–1061, May 2007.
- [17] M. Köstinger, M. Hirzer, P. Wohlhart, P. M. Roth, and H. Bischof, "Large scale metric learning from equivalence constraints," in *Proc. IEEE Conf. CVPR*, Jun. 2012, pp. 2288–2295.
- [18] Z. Li, S. Chang, F. Liang, T. S. Huang, L. Cao, and J. R. Smith, "Learning locally-adaptive decision functions for person verification," in *Proc. IEEE Conf. CVPR*, Jun. 2013, pp. 3610–3617.
- [19] M. Hirzer, P. M. Roth, and H. Bischof, "Person re-identification by efficient impostor-based metric learning," in *Proc. IEEE 9th Int. Conf. AVSS*, Sep. 2012, pp. 203–208.
- [20] M. Dikmen, E. Akbas, T. S. Huang, and N. Ahuja, "Pedestrian recognition with a learned metric," in *Proc. 10th ACCV*, 2011, pp. 501–512.
- [21] S. Yan, D. Xu, B. Zhang, H.-J. Zhang, Q. Yang, and S. Lin, "Graph embedding and extensions: A general framework for dimensionality reduction," *IEEE Trans. Pattern Anal. Mach. Intell.*, vol. 29, no. 1, pp. 40–51, Jan. 2007.
- [22] R. Zhao, W. Ouyang, and X. Wang, "Person re-identification by salience matching," in *Proc. IEEE ICCV*, Dec. 2013, pp. 2528–2535.
- [23] I. Kviatkovsky, A. Adam, and E. Rivlin, "Color invariants for person re-identification," *IEEE Trans. Pattern Anal. Mach. Intell.*, vol. 35, no. 7, pp. 1622–1634, Jul. 2013.
- [24] N. Martinel, A. Das, C. Micheloni, and A. K. Roy-Chowdhury, "Re-identification in the function space of feature warps," *IEEE Trans. Pattern Anal. Mach. Intell.*, vol. 37, no. 8, pp. 1656–1669, Aug. 2015.
- [25] S. Liao and S. Z. Li, "Efficient PSD constrained asymmetric metric learning for person re-identification," in *Proc. IEEE Int. Conf. Comput. Vis.*, 2015, pp. 3685–3693.
- [26] D. Tao, L. Jin, Y. Wang, and X. Li, "Person re-identification by minimum classification error-based KISS metric learning," *IEEE Trans. Cybern.*, vol. 45, no. 2, pp. 242–252, Feb. 2015.
- [27] S. Liao, Y. Hu, X. Zhu, and S. Z. Li, "Person re-identification by local maximal occurrence representation and metric learning," in *Proc. IEEE Conf. CVPR*, Jun. 2015, pp. 2197–2206.
- [28] F. Xiong, M. Gou, O. Camps, and M. Szaier, "Person re-identification using kernel-based metric learning methods," in *Proc. 13th ECCV*, 2014, pp. 1–16.
- [29] S. Paisitkriangkrai, C. Shen, and A. van den Hengel, "Learning to rank in person re-identification with metric ensembles," in *Proc. IEEE Conf. Comput. Vis. Pattern Recognit.*, 2015, pp. 1846–1855.
- [30] G. Lisanti, I. Masi, A. D. Bagdanov, and A. Del Bimbo, "Person re-identification by iterative re-weighted sparse ranking," *IEEE Trans. Pattern Anal. Mach. Intell.*, vol. 37, no. 8, pp. 1629–1642, Aug. 2014.
- [31] D.-N. T. Cong, C. Achard, and L. Khoudour, "People re-identification by classification of silhouettes based on sparse representation," in *Proc. 2nd IPTA*, Jul. 2010, pp. 60–65.
- [32] S. J. Pan, I. W. Tsang, J. T. Kwok, and Q. Yang, "Domain adaptation via transfer component analysis," *IEEE Trans. Neural Netw.*, vol. 22, no. 2, pp. 199–210, Feb. 2011.
- [33] B. Geng, D. Tao, and C. Xu, "DAML: Domain adaptation metric learning," *IEEE Trans. Image Process.*, vol. 20, no. 10, pp. 2980–2989, Oct. 2011.
- [34] M. Xiao and Y. Guo, "Feature space independent semi-supervised domain adaptation via kernel matching," *IEEE Trans. Pattern Anal. Mach. Intell.*, vol. 37, no. 1, pp. 54–66, Jan. 2014.
- [35] W.-S. Zheng, S. Gong, and T. Xiang, "Towards open-world person re-identification by one-shot group-based verification," *IEEE Trans. Pattern Anal. Mach. Intell.*, 2015, doi: 10.1109/TPAMI.2015.2453984.
- [36] A. J. Ma, P. C. Yuen, and J. Li, "Domain transfer support vector ranking for person re-identification without target camera label information," in *Proc. ICCV*, Dec. 2013, pp. 3567–3574.
- [37] L. Ma, X. Yang, and D. Tao, "Person re-identification over camera networks using multi-task distance metric learning," *IEEE Trans. Image Process.*, vol. 23, no. 8, pp. 3656–3670, Aug. 2014.
- [38] P. M. Roth, M. Hirzer, M. Köstinger, C. Beleznaï, and H. Bischof, "Mahalanobis distance learning for person re-identification," in *Person Re-Identification*, S. Gong, M. Cristani, S. Yan, and C. C. Loy, Eds. London, U.K.: Springer, 2014, pp. 247–267.
- [39] L. An, M. Kafai, S. Yang, and B. Bhanu, "Reference-based person re-identification," in *Proc. 10th AVSS*, Aug. 2013, pp. 244–249.
- [40] L. An, M. Kafai, S. Yang, and B. Bhanu, "Person re-identification with reference descriptor," *IEEE Trans. Circuits Syst. Video Technol.*, no. 99, Mar. 2015.
- [41] L. An, S. Yang, and B. Bhanu, "Person re-identification by robust canonical correlation analysis," *IEEE Signal Process. Lett.*, vol. 22, no. 8, pp. 1103–1107, Aug. 2015.

- [42] K. Liu, Z. Zhao, and A. Cai, "Datum-adaptive local metric learning for person re-identification," *IEEE Signal Process. Lett.*, vol. 22, no. 9, pp. 1457–1461, Sep. 2015.
- [43] W. Li and X. Wang, "Locally aligned feature transforms across views," in *Proc. CVPR*, Jun. 2013, pp. 3594–3601.
- [44] Y.-C. Chen, W.-S. Zheng, and J. Lai, "Mirror representation for modeling view-specific transform in person re-identification," in *Proc. IJCAI*, 2015, pp. 3402–3408.
- [45] A. Mignon and F. Jurie, "CMML: A new metric learning approach for cross modal matching," in *Proc. ACCV*, Nov. 2012, pp. 1–14.
- [46] H. H. Bauschke and J. M. Borwein, "Joint and separate convexity of the Bregman distance," *Stud. Comput. Math.*, vol. 8, pp. 23–36, 2001, doi: 10.1016/S1570-579X(01)80004-5.
- [47] S. Si, D. Tao, and B. Geng, "Bregman divergence-based regularization for transfer subspace learning," *IEEE Trans. Knowl. Data Eng.*, vol. 22, no. 7, pp. 929–942, Jul. 2010.
- [48] D. Gray, S. Brennan, and H. Tao, "Evaluating appearance models for recognition, reacquisition, and tracking," in *Proc. VS-PETS Workshop*, 2007, pp. 1–7.
- [49] W. Li, R. Zhao, and X. Wang, "Human reidentification with transferred metric learning," in *Proc. ACCV*, 2012, pp. 31–44.
- [50] D. S. Cheng, M. Cristani, M. Stoppa, L. Bazzani, and V. Murino, "Custom pictorial structures for re-identification," in *Proc. BMVC*, 2011, pp. 1–11.
- [51] A. Das, A. Chakraborty, and A. K. Roy-Chowdhury, "Consistent re-identification in a camera network," in *Computer Vision*. Zurich, Switzerland: Springer, 2014, pp. 330–345.
- [52] W.-S. Zheng, S. Gong, and T. Xiang, "Associating groups of people," in *Proc. BMVC*, 2009, pp. 23.1–23.11.
- [53] W. R. Schwartz and L. S. Davis, "Learning discriminative appearance-based models using partial least squares," in *Proc. 22nd Brazilian Symp. Comput. Graph. Image Process.*, Oct. 2009, pp. 322–329.
- [54] T. De Bie and B. De Moor, "On the regularization of canonical correlation analysis," in *Proc. Int. Symp. ICA BSS*, 2003, pp. 785–790.
- [55] X. Zhou, N. Cui, Z. Li, F. Liang, and T. S. Huang, "Hierarchical Gaussianization for image classification," in *Proc. ICCV*, Sep./Oct. 2009, pp. 1971–1977.
- [56] N. Martinel and C. Micheloni, "Re-identify people in wide area camera network," in *Proc. CVPR Workshop*, Jun. 2012, pp. 31–36.
- [57] L. Bazzani, M. Cristani, and V. Murino, "Symmetry-driven accumulation of local features for human characterization and re-identification," *Comput. Vis. Image Understand.*, vol. 117, no. 2, pp. 130–144, 2013.
- [58] T. Avraham, I. Gurvich, M. Lindenbaum, and S. Markovitch, "Learning implicit transfer for person re-identification," in *Computer Vision*. Berlin, Germany: Springer, 2012.



Ying-Cong Chen received the B.Sc. degree from Sun Yat-sen University, Guangzhou, China, in 2013, where he is currently pursuing the master's degree.

His current research interests include computer vision and machine learning.



Wei-Shi Zheng received the Ph.D. degree in applied mathematics from Sun Yat-Sen University, Guangzhou, China, in 2008.

He is currently a Professor with Sun Yat-sen University. He had been a Post-Doctoral Researcher on the EU FP7 SAMURAI Project at the Queen Mary University of London, London, U.K., and an Associate Professor at Sun Yat-sen University after that. He has now published more than 80 papers, including more than 40 publications in main journals (TPAMI, TNN, TIP, TSMC-B, and PR) and top conferences (ICCV, CVPR, IJCAI, and AAAI). He has joined the organization of four tutorial presentations in ACCV 2012, ICPR 2012, ICCV 2013, and CVPR 2015, along with other colleagues. His current research interests include person/object association and activity understanding in visual surveillance. He has joined Microsoft Research Asia Young Faculty Visiting Programme.

Dr. Zheng is a recipient of Excellent Young Scientists Fund of the National Natural Science Foundation of China, and a recipient of the Royal Society-Newton Advanced Fellowship.

Dr. Zheng is a recipient of Excellent Young Scientists Fund of the National Natural Science Foundation of China, and a recipient of the Royal Society-Newton Advanced Fellowship.



Jian-Huang Lai received the M.Sc. degree in applied mathematics and the Ph.D. degree in mathematics from Sun Yat-sen University, Guangzhou, China, in 1989 and 1999, respectively.

He is currently a Professor with the School of Information Science and Technology, Sun Yat-sen University. He has authored over 100 scientific papers in international journals and conferences on image processing and pattern recognition, e.g., the IEEE TRANSACTIONS ON PATTERN ANALYSIS AND MACHINE INTELLIGENCE, the IEEE TRANSACTIONS ON NEURAL NETWORKS, the IEEE TRANSACTIONS ON IMAGE PROCESSING, the IEEE TRANSACTIONS ON SYSTEMS, MAN, AND CYBERNETICS—PART B, *Pattern Recognition*, the IEEE International Conference on Computer Vision, the Computer Vision and Pattern Recognition Conference, and the IEEE International Conference on Data Mining. His current research interests include digital image processing, pattern recognition, multimedia communication, and wavelet and its applications.

His current research interests include digital image processing, pattern recognition, multimedia communication, and wavelet and its applications.



Pong C. Yuen received the B.Sc. (Hons.) degree in electronics engineering from the City Polytechnic of Hong Kong, Hong Kong, in 1989, and the Ph.D. degree in electrical and electronic engineering from The University of Hong Kong, Hong Kong, in 1993.

He joined Hong Kong Baptist University, Hong Kong, in 1993, where he is currently a Professor and the Head of the Department of Computer Science. In 1998, he spent a six-month sabbatical leave with the University of Maryland Institute for Advanced Computer Studies, University of Maryland, College Park, MD, USA. From 2005 to 2006, he was a Visiting Professor with the Graphics, Vision and Robotics Laboratory, INRIA Rhône-Alpes, Montbonnot-Saint-Martin, France. He was the Director of the Croucher Advanced Study Institute on biometric authentication in 2004 and biometric security and privacy in 2007. His current research interests include video surveillance, human face recognition, biometric security, and privacy.

Dr. Yuen serves as a Hong Kong Research Grant Council Engineering Panel Member. He was a recipient of the University Fellowship to visit The University of Sydney, Sydney, NSW, Australia, in 1996. He has been actively involved in many international conferences as an Organizing Committee Member or a Technical Program Committee Member. He was the Track Co-Chair of the International Conference on Pattern Recognition in 2006, and the Program Co-Chair of the IEEE Fifth International Conference on Biometrics: Theory, Applications and Systems in 2012. He is an Editorial Board Member of *Pattern Recognition*, and an Associate Editor of the IEEE TRANSACTIONS ON INFORMATION FORENSICS AND SECURITY and the *SPIE Journal of Electronic Imaging*.